J Nanopart Res (2020) 22: 219
https://doi.org/10.1007/s11051-020-04932-5

RESEARCH PAPER

Superparamagnetic graphene oxide/magnetite nanocomposite delivery system for doxorubicin-induced distinguished tumor cell cycle arrest and apoptosis

Mohamed L. Salem · Ali Gemeay · Soha Gomaa · Maha A. Aldubayan · Lobna Assy

Received: 30 January 2020 / Accepted: 25 June 2020 / Published online: 22 July 2020

Abstract By taking the advantage of supraparamagnetic graphene oxide (GO/Fe_3O_4) hybrid nanocomposite, as a drug delivery system with high thermal conductivity without altering its anti-tumor efficacy, this study aimed to investigate the behavior of doxorubicin (DOX) loaded onto GO/Fe_3O_4 as passive (GO/Fe_3O_4/DOX) or with folic acid (FA) as active (GO/Fe_3O_4/FA/DOX) hybrid form before and after external exposure to infrared radiation (IR), as a hyperthermia source. In addition to investigation of its anti-tumor actions and the associated cardiotoxicity effect, the conjugates were characterized by using TEM, FT-IR, and TGA analysis. Ehrlich ascites carcinoma (EAC) breast cancer cell line was used to assess the anti-tumor effects of these conjugates in vivo. The results confirmed the nanosize of conjugates, which showed high loading capacity surface area for DOX reaching up to 90%. Although the conjugates showed strong anti-tumor effects similar to those of DOX, they expressed different impacts on cell cycle and apoptosis of EAC cells. Additionally, when the conjugates were stimulated with IR, the level of creatine kinase-MB (CK-MB) as a cardiac biomarker was close to normal level. In conclusion, active (GO/Fe_3O_4/FA/DOX) hybrid form in combination with brief hyperthermia induces anti-tumor effect with less cardiotoxicity. Further studies are needed to optimize the beneficial effects of this kind of hyperthermia and to understand the underlying mechanisms.

Keywords Anti-tumor · Apoptosis · Cardiotoxicity · Cell cycle · Doxorubicin · Ehrlich ascites carcinoma · Hyperthermia · Superparamagnetic.

This article is part of the Topical Collection: *Nanotechnology in Arab Countries*, *Guest Editor*, *Sherif El-Eskandarany*

M. L. Salem · S. Gomaa · L. Assy (✉)
Immunology and Biotechnology Unit, Department of Zoology, Faculty of Science, Tanta University, Tanta, Egypt
e-mail: lobnaismailassy@gmail.com

M. L. Salem · L. Assy
Center of Excellence in Cancer Research, Tanta University, Teaching Hospital, Tanta University, Tanta, Egypt

A. Gemeay
Department of Chemistry, Faculty of Science, Tanta University, Tanta, Egypt

M. A. Aldubayan
Pharmacology and Toxicology Department, College of Pharmacy, Qassim University, Buraydah, Saudi Arabia

Introduction

Graphene oxide (GO) is a single atom thick sheet of sp^2 hybridized carbon atoms arranged in a hexagonal lattice, with remarkable physical and chemical characteristics including high mechanical properties, large surface area, and good thermal and electrical conductivity (Feng and Liu 2011; Muazim and Hussain 2017; Sanchez et al. 2012). Superparamagnetic graphene oxide (GO/Fe_3O_4) nanoparticles, as hybrid nanocomposite of GO and Fe_3O_4, are widely recognized for their safety and effectiveness in treating cancer relative to conventional forms of therapy (Hervault and Thanh 2014). One attractive behavior is the aptitude of Fe_3O_4 controlled drug

delivery, which outcomes from non/covalent dynamic bonding interactions, e.g., hydrogen bonding, π-π stacking, hydrophobic, and electrostatic interactions. The stimuli release is responded by temperature, pH, ultraviolet or visible lights, chemical substances, or electric fields (Mirhosseini et al. 2017; Siriviriyanun et al. 2015). Releasing of loaded chemotherapy drug from a delivery system depends on pH which varies from 7.4 in normal cells to 6.8 in extracellular microenvironment of solid tumors or between 5.0 and 6.5 in endosomal microenvironment of cancer cells (Su et al. 2011).

Under hyperthermia conditions, the nuclear membrane and the cytoskeletal assemblies are disrupted resulting in further disruption in the metabolic signaling processes, protein denaturation, and membrane blabbing. These events finally result in the apoptosis coinciding with the production of heat-shock proteins and other immunostimulants (Sahu et al. 2013). Because of their rapid metabolic rates, tumor cells are regarded as more vulnerable to the abovementioned hyperthermia effects (Dickerson et al. 2008). The latter would explain the potent anti-tumor effects obtained in patients upon their exposure to hyperthermia in the range of 39 to 45 °C, which was found to damage and kill cancer cells with minimal injury to the surrounding normal tissues (vander 2002).

Fe_3O_4 nanoparticles had the ability to absorb near-infrared (IR) light, which is converted into heat for the use in photothermal therapy. For instance, GO/Fe_3O_4 was found to induce ~ 90% decrease in cancer cell viability after using a 2 W cm^{-2} laser as the irradiation source for 5 min (Ma et al. 2012a). Interestingly, reduced GO/Fe_3O_4 conjugated with polyethylene glycol (PEG) achieved full ablation of 4T1 breast tumor in mice within 24 h after using a 0.5 W cm^{-2} laser as irradiation source (Yang et al. 2012). The main advantage of GO/Fe_3O_4-based hyperthermia treatment is the synergistic improvement in hyperthermic properties due to the high thermal conductivity of GO (Chen et al. 2014). The high infrared absorption capacity of GO allows photothermal effects to be exploited for localized cell killing through hyperthermia, where the infrared light is applied only to the area being targeted (Feng et al. 2014; Ma et al. 2012b).

Given that GO/Fe_3O_4 has strong thermal conductivity property, this study is aimed to load DOX onto GO/Fe_3O_4 with or without folic acid (FA) in the presence of infrared light source and to compare its anti-tumor effects with those of free DOX. Our data concluded that combination of GO/Fe_3O_4/FA nanocomposite and hyperthermia results in potential anti-tumor effects with minimal cardiotoxicity.

The active form of GO/Fe_3O_4 which could target cancer cells through certain receptors can be used as molecular signature cancer cells (Bhatia 2016) as transferrin (Daniels et al. 2006) and folic acid (FA) (Licciardi et al. 2006), through receptor-mediated endocytosis (Stella et al. 2000).

Materials and methods

Experimental animals

Female Swiss albino mice (6 weeks old and weighed 20 ± 3 g) were obtained from Company for Biological Products and Vaccines (VACSERA), Cairo, Egypt. All mice were housed at the animal unit, Zoology Department, Faculty of Science, Tanta University, Egypt, upon the approval of the institutional ethical committee (IA-CUC-SCI-TU-0071). All animals were housed under the same environmental conditions for 1 week before experimentation for acclimatization. Mice were housed under standard laboratory conditions (temperature 22 ± 2 °C; 12-h light-dark cycle) and kept in plastic cages with free access to the commercial basal food and water.

Reagents and antibodies

Graphite powder (~ 60 meshes, 98% purity), ferric chloride, ferrous sulfate, HCl, sulfuric acid, orthophosphoric acid, potassium permanganate, hydrogen peroxide, hydrazine monohydrate, phosphate buffer, and sterile PBS were purchased from LOBA Chemie, India. Propidium iodide (PI) and annexin V used for cell cycle and apoptosis analysis were purchased from BD Biosciences, USA.

Tumor cell line

Ehrlich ascites carcinoma (EAC) cell was obtained from the National Cancer Institute (NCI), Cairo, Egypt, and maintained in the ascitic form by sequential passages in female Swiss albino mice (obtained from NCI, Cairo, Egypt) by means of biweekly intraperitoneal (i.p.) injection of 2.5×10^6 tumor cells/mouse suspended in

0.1 ml PBS. In certain experiments, mice with EAC were exposed to infrared (IR) radiation using an IR lamp with 250 W from Philips.

Synthesis of GO

Graphene oxide (GO) was firstly synthesized by oxidation of natural graphite powder according to the modified Hammer's method (Marcano et al. 2010). Typically, 360 ml of H_2SO_4 was mixed with 40 ml of H_3PO_4 and then, 3 g of graphite powder was added. After a quiet stirring, 18 g $KMnO_4$ was added gradually producing a slight exothermic ~35–40 °C. The reaction was then warmed to 50–55 °C and stirred overnight. After the suspension color change from black to brown, the reaction was cooled to room temperature before it was transferred onto cold water 500 ml with 5 ml of 30% *v*/*v* H_2O_2. After that, the mixture was centrifuged at 6000 rpm. For work-up, the mixture was then washed in sequence with 100 ml of 30% HCl, demineralized water numerous times, and the supernatant was decanted away after being checked for sulfate, phosphate, and chloride ions. The remaining solid material was dried overnight at 60 °C, obtaining ~5 g of GO powder.

Synthesis of GO/Fe_3O_4 conjugate

Initially, 0.5 g of GO was dispersed in 100 ml distilled water by stirring. The dispersion was exfoliated by sonication to obtain evenly distributed GO sheets. The exfoliated GO dispersion was transferred into a round bottom flask followed by addition of $FeCl_3$ (6.5 g) and $FeSO_4$ (3.04 g) in 250 ml of distilled water and the pH was adjusted at 10 using NH_4OH solution. The resultant mixture was heated up to 80 °C with continuous stirring. Finally, the resultant black solid particles were separated by an external magnet and washed several times by water and ethanol and finally dried at 80 °C.

Synthesis of GO/Fe_3O_4/FA conjugate

Firstly, 0.5 g of GO/Fe_3O_4 was dispersed in 100 ml of distilled water in the ultrasonic bath for 1 h. Then, 0.5 g of FA was dissolved in 100 ml of distilled water. Finally, few drops of hydrazine monohydrate were added until complete solubility of FA. Therefore, the FA acidic solution was added to GO/Fe_3O_4 suspension and stirred for 24 h at room temperature. After the conjugating reaction, the suspension was ultra-centrifuged at 12,000 rpm and the precipitates were washed with DMSO three times and then dispersed into distilled water. The resulting GO/Fe_3O_4/FA was further purified with several ultracentrifugations and redispersion cycles. The absorbance of the FA was measured at λ_{max} = 360 nm. The loading capacity was calculated using Eq. (1):

$$\text{Loading}\% = \frac{C_{0=} - C_{\text{sup}}}{m_{\text{Go}}} \times 100 \quad (1)$$

where C_o represents the initial concentration of FA, C_{sup} the concentration of FA in the supernatant after reaction, and m_{GO} the mass of GO.

Loading of DOX onto GO/Fe_3O_4 or GO/Fe_3O_4/FA

Typically, 0.2 g of GO/Fe_3O_4 was suspended in 100 ml of PBS (pH = 7.4) and incubated in ultrasonic bath for 1 h at room temperature. The 10 ml of DOX solution of 50 mg/25 ml was added and the mixture was stirred in dark overnight. The mixture was centrifuged at 6000 rpm for 10 min. The particles were washed several times with water and dried overnight. The UV-Vis absorption spectra of the initial solution of DOX and the supernatant at λ_{max} = 480 nm were measured. The same procedure was followed for loading of DOX onto GO/Fe_3O_4/FA. The loading capacity was determined using the equation above used in case of the active forms.

In vivo anti-tumor effects of GO conjugates

Naïve female Swiss albino mice from VACSERA (Cairo, Egypt) were implanted with i.p. injection of $2.5 \times 10_5$ EAC cells/mouse and then divided randomly into the designated groups (n = 6/group). One day after EAC cell injection, mice were treated with PBS as control or administered with 300 μl DOX (15 mg/kg), and the prepared conjugates (GO/Fe_3O_4/DOX, GO/Fe_3O_4/FA/DOX, GO/Fe_3O_4/DOX + IR, and GO/Fe_3O_4/FA/DOX + IR) as, concentration of DOX in the conjugates was adjusted at 15 mg/kg in a suspension form. IR radiation was localized on EAC-bearing mice abdomen for 3 min with a distance of 30 cm. All mice were sacrificed on day 10 post-EAC inoculations by cervical dislocation. Prior to the scarifying, blood samples were collected from retro-orbital plexus and proceeded for hematological analysis using a Nihon Kohden automated

hematology analyzer (model MEK-6318K, Japan). The total number of EAC cells in the peritoneal exudate cells of each mouse was calculated by Trypan blue exclusion using hemocytometer.

Measuring cell cycle of EAC cells by flow cytometry

EAC cells were harvested from EAC-bearing mice previously treated with conjugates. EAC cells were prepared at a concentration of 2×10^6 cells/ml, washed twice with ice-cold PBS, and fixed with 70% ethanol at 4 °C overnight. The fixed cells were re-suspended in 300–500 μl PI/Triton X 100 staining solution (1000 μl of 0.1% Triton + 40 μl PI + 20 μl RNAse), for 30 min at 37 °C in the dark. The cells were then centrifuged at 1000×*g*, and the number of cells at the different phases of the cell cycle was analyzed using flow cytometry (BD FACSCanto II flow cytometry, BD Biosciences, USA) and the data were analyzed using BD FACS Diva software.

Measuring apoptosis of EAC cells by flow cytometry

EAC cells were collected from EAC-bearing mice previously treated with conjugates. EAC cells were washed twice with ice-cold PBS, the cell density was calculated, and the cells were re-suspended in 1× annexin-binding buffer to obtain a final density of 1×10^6 cells/ml. Then, 100 μl of the cell suspension was placed into 1.5-ml Eppendorf tubes and 5 μl annexin V-fluorescein isothiocyanate (FITC) and 1 μl PI (100 μg/ml) working solution were added. Stained EAC cells were then incubated at room temperature for 15 min followed by addition of 400 μl of 1× annexin-binding buffer with gentle mixing; then, the samples were kept on ice. The cells were then analyzed by flow cytometry.

Measuring CK-MB activity

CK-MB activity was detected in the sera of EAC-bearing mice at 450 nm, using Mouse Creatine Kinase MB isoenzyme kit.

Statistical analysis

Statistical analysis was performed using the GraphPad Prism (GraphPad Software, Inc., San Diego, CA) to analyze the obtained numerical data and *p* values. Data were represented as mean ± SE ($n = 3$). $*p \leq 0.05$, $**p \leq 0.01$, $***p \leq 0.001$, and $****p \leq 0.0001$ are statistically significant comparisons of control group and another treated group.

Results

Loading capacity of DOX onto GO/Fe_3O_4 or GO/Fe_3O_4/FA

The chemical structure of exfoliated GO sheets could increase the adsorption percentage of DOX through π-π stacking. To determine the saturation levels of DOX loading onto as prepared GO/Fe_3O_4, and GO/FA/Fe_3O_4, solutions were added with different amounts of DOX at pH 8.0. After removal of excess unbound DOX, the loading efficacy of DOX on GO/Fe_3O_4 composite was 94% as passive and 92% as active in the presence of folic acid (FA) which loaded by 88% on GO/Fe_3O_4 composite as shown in Fig. 1.

Transmission electron microscope images

The morphology of GO, GO/Fe_3O_4/DOX, and GO/Fe_3O_4/FA/DOX was characterized by transmission electron microscope (TEM). Figure 2 demonstrates the representative view of freestanding GO nanosheets. It shows a stacked and rippled structure, as a result of

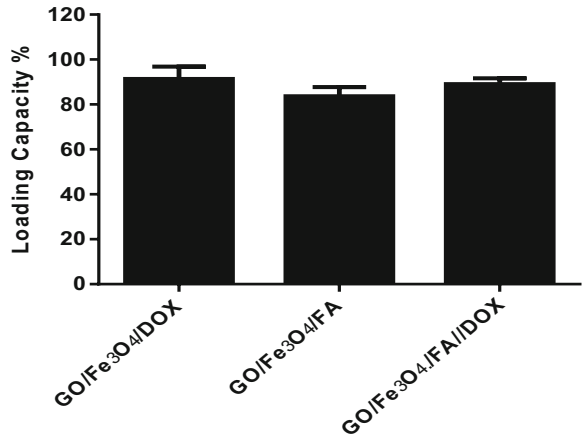

Fig. 1 Loading capacity of GO/Fe_3O_4 hybrid for DOX, FA, or FA and DOX. GO/Fe_3O_4 hybrid was prepared and loaded with DOX (0.5 mg/ml) or FA (1 mg/ml) or with combination of DOX and FA (0.5 mg/ml + 1 mg/ml), for 24 h at room temperature. The suspension was then ultra-centrifuged and the absorbance was measured after the conjugation at λ_{max} for DOX and FA at 480 and 360 nm, respectively. The data are represented by the average of triplicates experiments

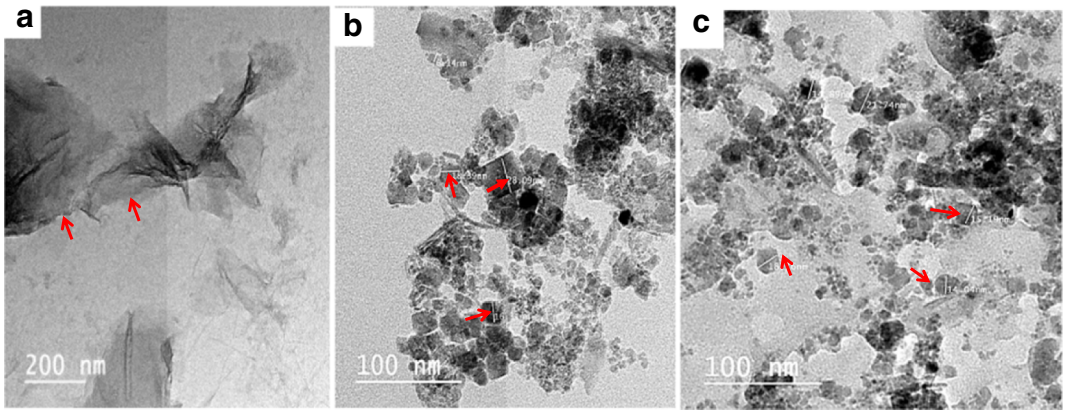

Fig. 2 TEM images of the GO/Fe_3O_4 hybrid after conjugation with GO/Fe_3O_4 hybrid for DOX, FA, or FA and DOX. GO/Fe_3O_4 hybrid was prepared and loaded as described previously in Fig. 1. **a** GO sheet alone as represented as layers as indicated by arrows. **b** GO/Fe3O4/DOX hybrid conjugate in which Fe_3O_4 nanoparticles are distributed randomly on the sheet surface as indicated by the arrows. **c** GO/Fe_3O_4/FA/DOX hybrid conjugate shows only fe3o4 as a distributed dark particles, while DOX or FA appear as shadow

deformation upon the exfoliation and restacking process. Fe_3O_4 nanoparticles showed diameters of 5–13 nm and are distributed randomly on the surface and edges of GO nanosheets. The data showed also that the GO nanosheets were coated by Fe_3O_4 nanoparticles, which densely deposited on both sides of the GO nanosheets to form a sandwich-like composite structure. Of note, almost no free Fe_3O_4 nanoparticles were found outside the GO nanosheets even after intensive ultrasonication, indicating a strong interaction between Fe_3O_4 and GO.

FT-IR analysis of the conjugates

The FT-IR spectra of GO and GO/Fe_3O_4 hybrid are shown in Fig. 3. The peak at 1700 cm^{-1} corresponding to ν(C=O) of –COOH on the GO was shifted to 1550 cm^{-1} due to the formation of COO after coating with Fe_3O_4. The characteristic peak corresponding to the stretching vibration of Fe–O bond was also shifted to higher wave number of 700 cm^{-1} as compared with that of 570 cm^{-1} reported for the stretching mode of Fe–O in bulk Fe_3O_4, suggesting that Fe_3O_4 is bound to the –COO on the GO surface.

Thermogravimetric analysis of the conjugates

Thermogravimetric (TGA) analyses of the conjugates are shown in Fig. 4. GO/Fe_3O_4/DOX showed a total weight loss of 33 wt.% in 4 steps. The first weight loss of 7 wt.% at < 100 °C was observed which can be due to the loss of the residual or absorbed solvent. The large weight loss occurred at the onset of 385 °C with 12 wt.% which may be due to the breakdown of the –COOH group. When the temperature reached 800 °C, the weight of the composite remained at 67 wt.% and almost no weight loss occurred after this temperature, while for GO/Fe_3O_4/FA/DOX, the curve showed a weight loss in 5 steps with a total weight loss of 27 wt.%, which may be due to the breakdown of the –COO group. A weight loss of approximately 6% was observed between 280 and 320 °C, possibly due to the detachment of FA.

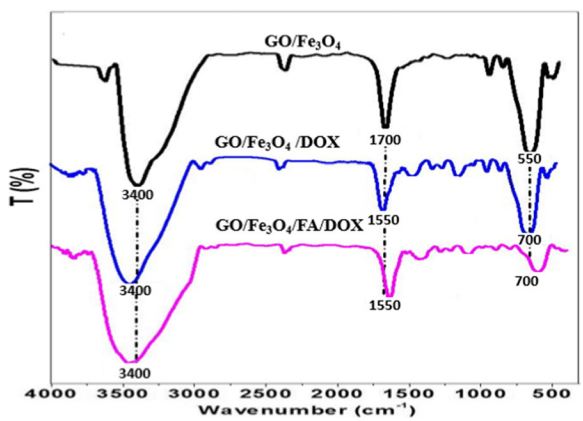

Fig. 3 FT-IR spectrum of GO/Fe_3O_4 hybrid after conjugation with DOX, FA or FA and DOX. GO/Fe3O4 hybrid was prepared and loaded as described previously in Fig. 1. The black line represents GO/Fe_3O_4 hybrid with the functional groups of GO and Fe_3O_4. The blue line represents GO/Fe_3O_4/DOX hybrid conjugate and the purple line represents GO/Fe_3O_4/FA/DOX hybrid conjugate. The peaks in each line reflect the main functional groups

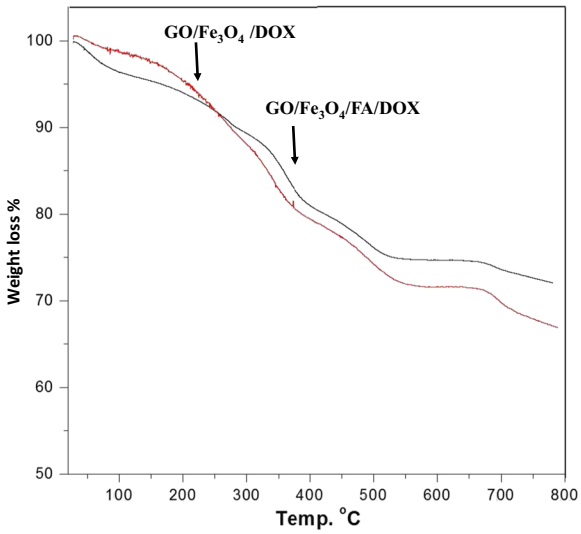

Fig. 4 TGA analysis of GO/Fe_3O_4 /DOX hybrid conjugate with or without FA. GO/Fe3O4 hybrid was prepared and loaded as described previously in Fig. 1. The red line shows GO/Fe_3O_4/DOX and the blue line shows GO/Fe_3O_4/FA/DOX hybrid conjugate forms

Further weight loss of 2% occurred between 500 and 600 °C, which may be due to detachment of DOX from the final conjugate.

Vibrating sample magnetometer analysis

The magnetic properties of GO–Fe_3O_4 at room temperature were characterized by using vibrating sample magnetometer (VSM). As shown in Fig. 5, the magnetization hysteresis loops of GO–Fe_3O_4 have S-like curves and the saturation magnetization values increased with the increment of Fe_3O_4 loading amount and equals 23 emu/g. The saturation magnetizations of our GO–Fe_3O_4 hybrids were much smaller when compared with those of pure bulk Fe_3O_4.

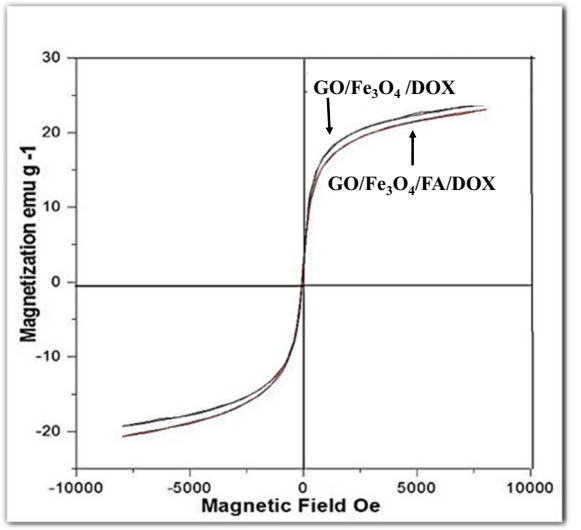

Fig. 5 Vibrating sample magnetometer (VSM) analysis of GO/Fe3O4 hybrid after conjugation with DOX, FA, or FA and DOX. GO/Fe3O4 hybrid was prepared and loaded as described previously in Fig. 1. The black line shows GO/Fe_3O_4/DOX and the red line shows GO/Fe_3O_4/FA/DOX hybrid conjugate forms

In vivo anti-tumor effect of conjugates

To evaluate the anti-tumor effects of the formed conjugates, mice were inoculated with EAC cells and treated 1 day later with each conjugate condition or with free DOX or PBS. Treatment with free DOX decreased the numbers of EAC cells to (5×10^6) as compared with control treated mice (187×10^6). Treatment with GO/Fe_3O_4/DOX or GO/Fe_3O_4/FA/DOX resulted in significant decrease of the numbers of EAC cells to 10×10^6 and 26×10^6, respectively. Treatment with GO/Fe_3O_4/DOX + IR or GO/Fe_3O_4/FA/DOX + IR resulted in significant decrease of the numbers of EAC cells to 17×10^6 and 9×10^6, respectively, as compared with treatment with IR alone (75×10^6) (Fig. 6).

Effect of conjugates on EAC cell cycle

Nuclear DNA content of EAC cells was analyzed using flow cytometry after treatment of EAC-bearing mice with GO/Fe_3O_4/DOX, GO/Fe_3O_4/FA/DOX, GO/Fe_3O_4/DOX + IR, and GO/Fe_3O_4/FA/DOX + IR (loaded with 15 mg/kg DOX) or with free DOX (15 mg/kg) as a reference drug. The results showed that the DNA content of EAC cells underwent different phases (subG, /G1, S, and G2M) of the cell cycle before mitotic division, and graphs of fractional DNA content (PI fluorescence, X-axis) versus cell counts (Y-axis) are shown in Fig. 7. The passive forms of the conjugates (GO/Fe_3O_4/DOX and GO/Fe_3O_4/DOX + IR) induced arrest of EAC cell cycle at early phases (G1 and GO). While the active forms of the conjugates (GO/Fe_3O_4/FA/DOX and GO/Fe_3O_4/FA/DOX + IR) induced arrest of EAC cell cycle at the late phases (S and G2M).

The cell cycle distribution of EAC cells from EAC-bearing mice treated with GO/Fe_3O_4/DOX or GO/Fe_3O_4/FA/DOX showed cell cycle arrest at G1 phase (54%) and S phase (69.7%), respectively. While those from mice treated with GO/Fe_3O_4/DOX + IR and GO/Fe_3O_4/FA/DOX + IR showed cell cycle arrest at S/GO

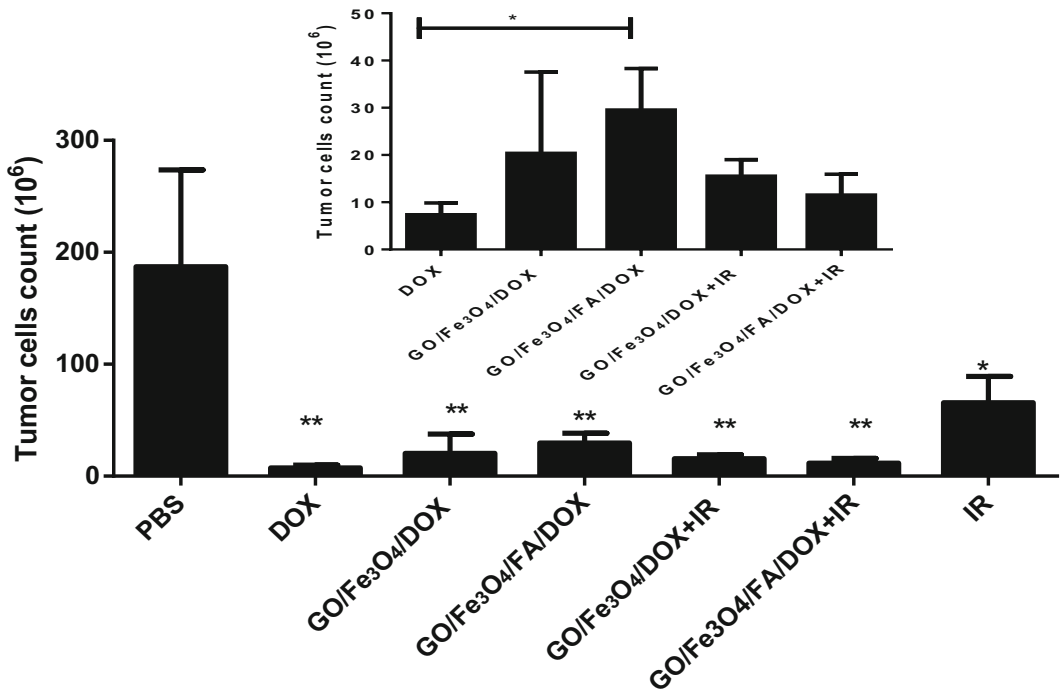

Fig. 6 Anti-tumor effects of GO/Fe_3O_4 hybrid conjugates on EAC-bearing mice. Mice were challenged i.p. with of EAC (2.5×10^5) cells on day 0. Then, divided into 7 groups and four groups (1–4) treated with PBS, DOX GO/Fe_3O_4/DOX, and GO/Fe_3O_4/FA/DOX, respectively, groups 5 and 6 treated with GO/Fe_3O_4/DOX and GO/Fe_3O_4/FA/DOX then had an external localized exposure of IR source for 3 min with a distance of 30 cm, additional EAC-bearing mice group exposure to IR only on day 1. All groups were sacrificed on day 10. EAC cells collected for count by Trypan blue exclusion. Data are represented as mean ± SE ($n = 6$). *$p \leq 0.05$ and **$p \leq 0.01$, statistically significant comparison between all treated groups and PBS group without treatment. The inset data represents the effect of GO/Fe_3O_4 hybrid forms with or without IR compared with free DOX

(61.5%) and at G2M (89.5%) phase, respectively. EAC cells from mice exposed to IR only showed cell cycle arrest at G1 (45%) as compared with free DOX which induced EAC cell cycle arrest at S/GO phase (40.4%) (Fig. 7).

Effect of treatment with conjugates on apoptosis of EAC cells

Early apoptotic, late apoptotic, and necrotic cell percentage of EAC cells was analyzed using flow cytometry

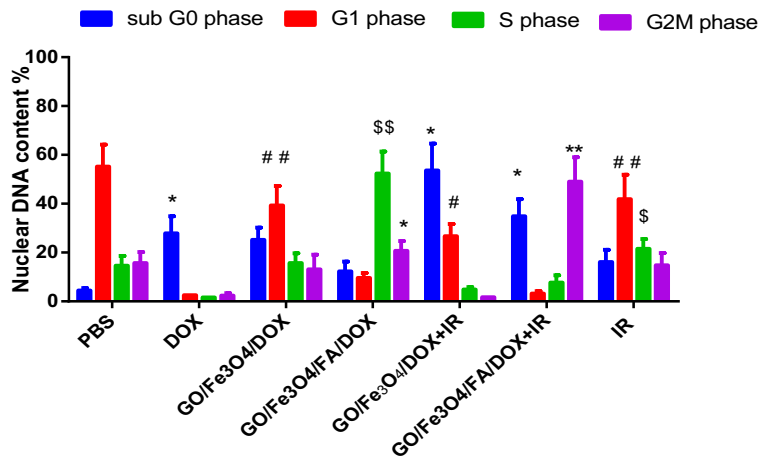

Fig. 7 Effect of GO/Fe_3O_4 hybrid conjugates with DOX, FA, or FA and DOX on EAC cell cycle. Mice were challenged i.p. as described previously in Fig. 5. EAC cells were harvested for cell cycle analysis by flow cytometry. Data are represented as mean ± SE ($n = 6$). *$p \leq 0.05$, **$p \leq 0.01$, statistically significant comparison between cell cycle phases of treated groups and PBS group without treatment

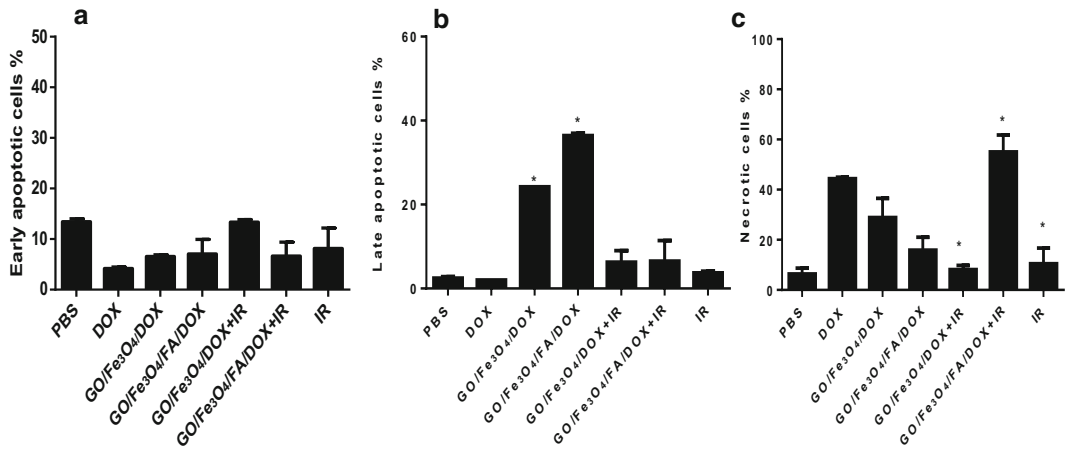

Fig. 8 Effect of GO/Fe_3O_4 hybrid conjugates with DOX, FA, or FA and DOX on EAC cell apoptosis. Mice were challenged i.p. as described previously in Fig. 5. EAC were harvested and counted and used for apoptosis analysis using annexin V and PI by flow cytometry. **a** Early apoptosis of EAC cells (Annexin$^+$PI$^-$), **b** late apoptosis (Annexin$^+$ PI$^+$), and **c** necrosis (Annexin$^-$PI$^+$). Data are represented as mean ± SE ($n = 6$) *$p \le 0.05$, **$p \le 0.01$, statistically significant of all treated groups as compared with PBS group without treatment

after treatment with GO/Fe_3O_4/DOX, GO/Fe_3O_4/FA/DOX, GO/Fe_3O_4/DOX + IR, or GO/Fe_3O_4/FA/DOX + IR and the phenotypic distributions of early apoptotic (Annexin$^+$PI$^-$), late apoptotic (Annexin$^+$PI$^+$), and necrotic (Annexin$^-$PI$^+$) cells are displayed in Fig. 8. The results showed that all conjugates induced similar effect on early apoptotic cells. Administration of GO/Fe_3O_4/FA/DOX or GO/Fe_3O_4/DOX increased late apoptotic cells to 36.40% and 24.20%, respectively, as compared with the control EAC group (2.4%), when DOX was 5%, while treatment with GO/Fe_3O_4/FA/DOX + IR induced a highly significant increase of necrotic cells to 55% as compared with the EAC group (6.3%) as compared with DOX treatment which induced (44%) of necrotic cells.

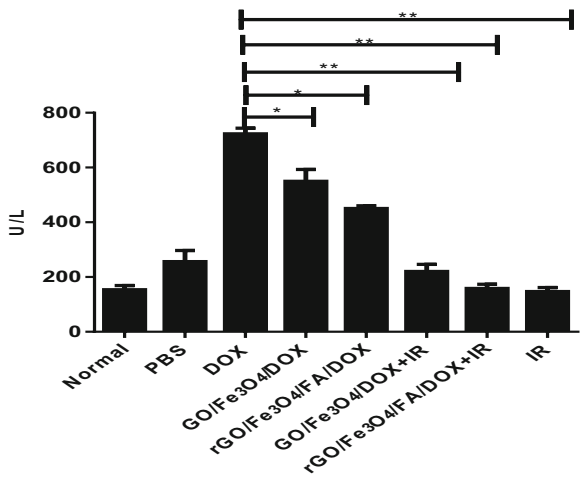

Fig. 9 Effect of GO/Fe_3O_4 hybrid conjugates with DOX, FA, or FA and DOX on cardiotoxicity. Mice were challenged i.p. as described previously in Fig. 5. CK-MB activity was determined on the collected sera at wavelength 450 nm. Data are represented as mean ± SE ($n = 6$). *$p \le 0.05$, **$p \le 0.01$, statistically significant comparison between all treated groups and the healthy normal group

Effect of treatment with GO conjugates on cardiotoxicity

Results in Fig. 9 revealed that CK-MB activity in sera of EAC-bearing mice showed highly significant increase in the untreated (257 μ/l) group as compared with the control mice without tumor (150 μ/l). Treatment of EAC-bearing mice with GO/Fe_3O_4/DOX or GO/Fe_3O_4/FA/DOX also showed high levels of CK-MB. Interestingly, however, treatment with GO/Fe_3O_4/DOX + IR (220 μ/l), GO/Fe_3O_4/FA/DOX + IR (153 μ/l), and IR alone (147 μ/l) decreased the elevated serum levels of CK-MB activity to a level close to its level in tumor-nonbearing mice.

Discussion

The present work primarily aims at fabricating a trifunctional material with abundant adsorption and drug delivery domains. The trifunctional material

contains graphene oxide, Fe_3O_4 nanoparticles, and folic acid (FA). The resultant Fe_3O_4/GO nanocomposites were synthesized via depositing Fe_3O_4 onto GO sheets by co-precipitation method, followed by loading DOX as passive form (GO/Fe_3O_4/DOX) or as an active form through loading of FA (GO/Fe_3O_4/FA/DOX). The function of FA was the binding with FA receptor in cancer cells. Chen et al. (2014) reported the importance of GO/Fe_3O_4 nanocomposite in hyperthermia applications for cancer cell treatment. In the present study, external infrared-radiation was used as a source of hyperthermia. The results revealed that the loading of DOX onto GO/Fe_3O_4 nanocomposite reached about 94%, which indicates that the conjugation of GO with Fe_3O_4 does not impact the loading of DOX onto GO. This data is consistent with a prior study which recorded over 90% of DOX loading over GO (Zhou et al. 2014). This conjugation could be explained at least in part mainly through π-π stacking interaction (Zhao et al. 2011), the interaction between GO and positively charged DOX molecules (Wu et al. 2013), as well as the expected formation of additional hydrogen bonding formation (Gong et al. 2018) between $–NH_2$ groups in DOX with GO as confirmed by FT-IR spectrum.

Moreover, testing the impact of the conjugation of FA with GO/Fe_3O_4 exhibited that the loading capacity of DOX onto GO/ Fe_3O_4 was decreased from 94 to 92% in the case of GO/Fe_3O_4/FA nanocomposite. Although this decrease is no significant difference, it is critical to be considered during drug dose calculations because it depends on available surface sites. This reduction in the loading capacity could be explained by the chemical manipulation of GO during its reduction to form r-GO/Fe_3O_4 and the removal of the majority of the oxygenated functional groups (Akhavan et al. 2012). Another explanation could be the competition between FA molecules and DOX on GO/Fe_3O_4 surface.

It is well known that particle size is crucial for biomedical applications during circulation and biodistribution inside living system. For nano medicine, particles having a size of less than 10 nm can be easily cleared from kidneys or through extravasation, while larger particles have adverse effect in diagnostic sensitivity and therapeutic efficacy and have higher tendency to be cleared by the reticuloendothelial system. Furthermore, TEM analysis of the conjugates showed that morphology of GO was stable after chemical manipulation by Fe_3O_4 or conjugation with DOX or FA. Our results showed that conjugation of DOX with GO/Fe_3O_4 in the presence or absence of FA does not interfere with the anti-tumor effect of DOX in vivo. Taken together, the data of this study confirmed the efficacy of GO to carry drugs even in a reduced form.

In this study, both of forms showed similar anti-tumor effect, indicating the superior effect of GO/Fe_3O_4 regardless of the exposure to IR. The anti-tumor effects of the passive and active forms of GO/Fe_3O_4 drug delivery systems in the present study showed that both forms had strong and almost similar anti-tumor effects. However, the active form (GO/Fe_3O_4/FA/DOX) had higher effect than the passive form (GO/Fe_3O_4/DOX). These results are in line with previous studies which showed that the anti-tumor effect of active GO is superior to those of the passive form against several tumors. For instance, the encapsulated hyaluronic acid-chitosan-g-poly-*N*-isopropylacrylamide (HACPN) GO/FA/DOX/HACPN showed higher anti-tumor efficacy against xenograft tumor MCF-7 (MCF-7/Luc cells) than its passive form (Fong et al. 2017). It has also been reported that GO/DOX (passive) nanosheets coated with an anti-angiogenic derivative of low-molecular-weight heparin (LHT7) showed the greatest anti-tumor effect in tumor-bearing mice (Shim et al. 2014). These superior effects of the active form could be explained as the conjugation of DOX onto GO/Fe_3O_4 drug delivery system was harder than that of the GO system.

Hyperthermia therapy is one of the means of interventional ablation since it can lead to killing the tumor by irradiation. However, due to the limited penetration of the radiation to the tissue, the use of photosensitizers in combination with IR is often required. GO has a good photothermal conversion effect which when it is combined with laser treatment can effectively produce overheating effect. The latter leads to tumor killing. Therefore, GO is considered to be efficient as the photosensitizer (Sahu et al. 2013).

Interestingly, measuring the anti-tumor effects of the two forms of GO/Fe_3O_4 drug delivery system combined with infrared-A lamp as a source of the hyperthermia showed that both forms had strong anti-tumor effects. However, the active form (GO/Fe_3O_4/FA/DOX + IR) had higher effect than the passive form (GO/Fe_3O_4/DOX + IR). These results could be explained as increasing the temperature more than 40 °C results in disruption of nuclear and cytoskeletal assemblies, protein denaturation, and the onset of or apoptosis caused by the

production of heat-shock proteins and other immunostimulants (Dickerson et al. 2008).

These results are in line with previous in vivo studies which showed that 980-nm laser combined with GO on pancreatic cancer cells can achieve higher therapeutic temperature and better therapeutic effect than laser alone (Wu et al. 2018). Another study showed that the combined GO-PEG-DOX photothermal treatment resulted in complete destruction of the tumors without weight loss or recurrence of tumors as compared with DOX alone or NGO-PEG photo-thermal treatment alone. More importantly, this combined treatment showed reduced drug side effects in comparison with free DOX. Folic acid (FA) was conjugated to the nanocomposite for more specific drug and heat delivery to tumor cell (Qin et al. 2013). While, the other study showed that tumors in mice treated by intratumorally injection of reduced GO combined with infrared laser irradiation became smaller and then were eradicated completely after a month (Yang et al. 2012). The anti-tumor effect of hyperthermia could be a result of direct effect of radiation only or the additive anti-tumor effects of the conjugate and radiation.

Although the mechanisms behind the beneficial anti-tumor effects of IR were not investigated in this study, several studies reported that hyperthermia can cause DNA fragmentation and the formation of double-strand breaks (Kong 2007; Kuhl 2000), which could arise from the inhibition of DNA repair mechanisms. However, it appears that nuclear protein damage may be the key factor rather than direct DNA damage itself. Nuclear proteins, in particular, appear to be very sensitive to hyperthermia and undergo aggregation (Sugahara et al. 2008). Elevated temperatures can increase the rates of biochemical reactions and this would increase cell metabolism, which should cause increased oxidative stress.

Several anticancer compounds demonstrate their growth inhibitory effect either by arresting the cell cycle at a specific checkpoint of cell cycle or by induction of apoptosis or a collective effect of both cycle arrest and apoptosis (Gerard and Karen 2001). As such, the impacts of the conjugates on these parameters were analyzed in the present study. Although all forms of the conjugates induced similar anti-tumor effect, they showed different profiles on tumor cell cycle. The passive form (GO/Fe_3O_4/DOX) arrested the tumor cell cycle at G0/G1, while the active form (GO/Fe_3O_4/FA/DOX) arrested the cell cycle at the S phase. Interestingly, the passive form GO/Fe_3O_4/DOX combined with IR induced tumor cell cycle arrest at subG0 phase which could be temporary cell cycle arrest of tumor cells and mitotic division could be processed after that. While, the active form GO/Fe_3O_4/FA/DOX + IR combined with IR induced tumor cell cycle arrest at G2M phase. The role of DOX in these variabilities could be excluded since it belongs to the class of cycle-phase nonspecific drugs which can kill tumor cells with a variety of cell cycles (Offelt and Visser 2015). The results of the previous studies indicated that nanomaterials may lead to cell cycle arrest at various phases (Kim et al. 2015; Patel et al. 2016). In line with our results, GO and rGO induce cell cycle arrest at the G0/G1 phase suggesting that GO causes more potent toxic effects than rGO (Khan et al. 2016; Linares et al. 2016).

With regard to apoptosis of EAC cells, the current study revealed that GO/Fe_3O_4/FA/DOX + IR treatment showed high increases in the numbers of EAC cell late apoptosis. While, GO/Fe_3O_4 FA/DOX caused more necrotic cells as compared with free DOX. These data suggest that the anti-tumor effects of the conjugates are mediated by both arresting tumor cell cycle both inducing apoptosis. These results were in line with the previous study which showed that GO/FA/DOX and GO/DOX induced apoptosis of MCF7 cells and multiple myelomas (Wu et al. 2014).

With regard to cardiotoxicity evaluation, CK-MB level from DOX-treated group showed the top level of significance, as DOX is known for its cardiotoxicity (Takemura and Fujiwara 2007; Zhao and Zhang 2017), as well as GO/Fe_3O_4/DOX and GO/Fe_3O_4 FA/DOX treatments induced a significantly associated cardiotoxicity. This result is in good agreement with the previous study as it is reported that iron nanoparticles lead to acute heart rate reduction in vivo (Iversen et al. 2013). Interestingly, conjugates GO/Fe3O4/DOX + IR and GO/Fe3O4 FA/DOX + IR in combination with localized exposure with IR were found to associate with less cardiac toxicity approximate as a normal healthy group.

In conclusion, active form of hybrid composite GO/Fe_3O_4FA/DOX + IR in combination with hyperthermia induces anti-tumor effect with less cardiotoxicity. Further studies are needed to optimize the beneficial effects of this kind of hyperthermia and to understand the underlying mechanisms.

Compliance with ethical standards

Conflict of interest The authors declare that they have no conflict of interest.

References

Akhavan O, Ghaderi E, Alireza A (2012) Size-dependent genotoxicity of graphene nanoplatelets in human stem cells. Biomaterials 33:8017–8025

Bhatia S (2016) Nanoparticles types, classification, characterization, fabrication methods and drug delivery applications in natural polymer drug delivery systems: nanoparticles, plants, and algae. Springer International Publishing, Switzerland, pp 33–93. https://doi.org/10.1007/978-3-319-41129-3_2

Chen Y et al (2014) Multifunctional graphene oxide-based triple stimuli-responsive. Nanotheranostics Adv Funct Mater 24: 4386–4396

Daniels TR, Delgado T, Rodriguez JA, Helguera G, Penichet ML (2006) The transferrin receptor part II: targeted delivery of therapeutic agents into cancer cells. Clin Immunol 121:159–176

Dickerson EB et al (2008) Gold nanorod assisted near-infrared plasmonic photothermal therapy (PPTT) of squamous cell carcinoma in mice. Cancer Lett 269:57–66. https://doi.org/10.1016/j.canlet.2008.04.026

Feng L, Li K, Shi X, Gao M, Liu J, Liu Z (2014) Smart pH-responsive nanocarriers based on nano-graphene oxide for combined chemo- and photothermal therapy overcoming drug resistance. Adv Healthcare Mater 3:1261–1271

Feng L, Liu Z (2011) Graphene in biomedicine: opportunities and challenges. Nanomedicine (Lond) 6:317–324. https://doi.org/10.2217/nnm.10.158

Fong YT, Chen CH, Chen JP (2017) Intratumoral delivery of doxorubicin on folate-conjugated graphene oxide by in-situ forming thermo-sensitive hydrogel for breast cancer. Therapy Nanomaterials (Basel) 7:388. https://doi.org/10.3390/nano7110388

Gerard EI, Karen VH (2001) Proliferation, cell cycle and apoptosis in cancer. Nature 411:342–348

Gong P et al (2018) Fluorinated graphene as an anticancer nanocarrier: an experimental and DFT study. Journal of Materials Chemistry B 6:2769–2777

Hervault A, Thanh NT (2014) Magnetic nanoparticle-based therapeutic agents for thermo-chemotherapy treatment of cancer. Nanoscale 6:11553–11573. https://doi.org/10.1039/c4nr03482a

Iversen NK et al (2013) Superparamagnetic iron oxide polyacrylic acid coated gamma-Fe2O3 nanoparticles do not affect kidney function but cause acute effect on the cardiovascular function in healthy mice. Toxicol Appl Pharmacol 266:276–288. https://doi.org/10.1016/j.taap.2012.10.014

Khan M et al (2016) Apoptosis inducing ability of silver decorated highly reduced graphene oxide nanocomposites in A549 lung cancer. Int J Nanomedicine 11:873–883. https://doi.org/10.2147/IJN.S100903

Kim KJ, Joe V, Kim MK, Lee SJ, Ryu YH, Cho DW, Rhie JW (2015) Silica nanoparticles increase human adipose tissue-derived stem cell proliferation through ERK1/2 activation. Int J Nanomedicine 10:2261–2272

Kong LJS (2007) Heat shock protein 70 inhibits the nuclear import of apoptosis inducing factor to avoid DNA fragmentation in TF-1 cells during erythropoiesis. FEBS Lett 58:109–117

Kuhl NMJKLR (2000) Heat shock-induced arrests in different cell cycle phases of rat C6-glioma cells are attenuated in heat shock-primed thermo tolerant cells. Cell Prolif 33:147–166

Licciardi M, Giammona G, Du J, Armes SP, Tang Y, Lewis AL (2006) New folate-functionalised biocompatible block copolymer micelles as potential anti-cancer drug delivery systems. Polymer 47:2946–2955. https://doi.org/10.1016/j.polymer.2006.03.014

Linares J, Matesanz MC, Feito MJ, Salavagione HJ, Martinez G, Gomez-Fatou M, Portoles MT (2016) Influence of the covalent immobilization of graphene oxide in poly(vinyl alcohol) on human osteoblast response. Colloids Surf B Biointerfaces 138:50–59. https://doi.org/10.1016/j.colsurfb.2015.11.035

Ma X et al (2012a) A functionalized graphene oxide-iron oxide nanocomposite for magnetically targeted drug delivery, photothermal therapy, and magnetic resonance imaging. Nano Research 5:199–212. https://doi.org/10.1007/s12274-012-0200-y

Ma XX, Tao HQ, Yang K, Feng LZ, Cheng L, Shi XZ (2012b) A functionalized graphene oxide-iron oxide nanocomposite for magnetically targeted drug delivery, photothermal therapy, and magnetic resonance imaging. Nano Res 5:199–212

Marcano DC et al (2010) Improved synthesis of graphene oxide. ACS Nano 4:4806–4814. https://doi.org/10.1021/nn1006368

Mirhosseini MM, Rahmati M, Zargarian SS, Khordad R (2017) Molecular dynamics simulation of functionalized graphene surface for high efficient loading of doxorubicin. J Mol Struct 1141:441–450. https://doi.org/10.1016/j.molstruc.2017.04.007

Muazim K, Hussain Z (2017) Graphene oxide—a platform towards theranostics. Mater Sci Eng C 76:1274–1288. https://doi.org/10.1016/j.msec.2017.02.121

Offelt SB, Visser KE (2015) Immune-mediated mechanisms influencing the efficacy of anticancer therapies. Trends Immunol 36:198–216. https://doi.org/10.1016/j.it.2015.02.006

Patel P, Kansara K, Senapati VA, Shanker R, Dhawan A, Kumar A (2016) Cell cycle dependent cellular uptake of zinc oxide nanoparticles in human epidermal cells. Mutagenesis 31: 481–490

Qin XC, Guo ZY, Liu ZM, Zhang W, Wan MM, Yang BW (2013) Folic acid-conjugated graphene oxide for cancer targeted chemo-photothermal therapy. J Photochem Photobiol B 120:156–162. https://doi.org/10.1016/j.jphotobiol.2012.12.005

Sahu A, Choi WI, Lee JH, Tae G (2013) Graphene oxide mediated delivery of methylene blue for combined photodynamic and photothermal therapy. Biomaterials 34:6239–6248. https://doi.org/10.1016/j.biomaterials.2013.04.066

Sanchez VC, Jachak A, Hurt RH, Kane AB (2012) Biological interactions of graphene-family nanomaterials: an interdisciplinary review. Chem Res Toxicol 25:15–34. https://doi.org/10.1021/tx200339h

Shim G, Kim JY, Han J, Chung SW, Lee S, Byun Y, Oh YK (2014) Reduced graphene oxide nanosheets coated with an anti-angiogenic anticancer low-molecular-weight heparin derivative for delivery of anticancer drugs. J Control Release 189:80–89

Siriviriyanun A, Popova M, Imae T, Kiew LV, Looi CY, Wong WF (2015) Preparation of graphene oxide/dendrimer hybrid carriers for delivery of doxorubicin. Chem Eng J 281:771–781. https://doi.org/10.1016/j.cej.2015.07.024

Stella B, Arpicco S, Peracchia MT, Desmaële D, Hoebeke J, Renoir M, D'Angelo J, Cattel L, Couvreur P (2000) Design of folic acid-conjugated nanoparticles for drug targeting. J Pharm Sci 89:1452–1464. https://doi.org/10.1002/1520-6017(200011)89:11<1452::aid-jps8>3.0.co;2-p

Su J, Chen F, Cryns V, Messersmith P (2011) Catechol polymers for pH-responsive targeted drug delivery to cancer cells. J Am Chem Soc 133:11850–11853

Sugahara T, van der Zee J, Kampinga HH, Vujaskovic Z, Kondo M, Ohnishi T, Li G, Park HJ, Leeper DB, Ostapenko V, Repasky EA, Watanabe M, Song CW (2008) Kadota Fund International Forum 2004. Application of thermal stress for the improvement of health, 15-18 June 2004, Awaji Yumebutai International Conference Center, Awaji Island, Hyogo, Japan. Final report. Int J Hyperthermia 24:123–140. https://doi.org/10.1080/02656730701883675

Takemura G, Fujiwara H (2007) Doxorubicin-induced cardiomyopathy from the cardiotoxic mechanisms to management. Prog Cardiovasc Dis 49:330–352. https://doi.org/10.1016/j.pcad.2006.10.002

Vander JZ (2002) Heating the patient: a promising approach? Ann Oncol 13:1173–1184

Wu J, Li Z, Li Y, Pettitt A, Zhou F (2018) Photothermal effects of reduced graphene oxide on pancreatic cancer. Technol Cancer Res Treat 17:1533034618768637. https://doi.org/10.1177/1533034618768637

Wu S, Zhao X, Cui Z, Zhao C, Wang Y, Du L, Li Y (2014) Cytotoxicity of graphene oxide and graphene oxide loaded with doxorubicin on human multiple myeloma cells. International Journal of Nanomedicine 9:1413–1421. https://doi.org/10.2147/IJN.S57946

Wu S, Zhao X, Li Y, du Q, Sun J, Wang Y, Wang X, Xia Y, Wang Z, Xia L (2013) Adsorption properties of doxorubicin hydrochloride onto graphene oxide: equilibrium. Kinetic and Thermodynamic Studies Materials (Basel) 6:2026–2042. https://doi.org/10.3390/ma6052026

Yang K et al (2012) Multimodal imaging guided photothermal therapy using functionalized graphene nanosheets anchored with magnetic nanoparticles. Adv Mater 24:1868–1872. https://doi.org/10.1002/adma.201104964

Zhao GX, Li JX, Wang XK (2011) Kinetic and thermodynamic study of 1-naphthol adsorption from aqueous solution to sulfonated graphene nanosheets. Chem Eng J 173:185–190

Zhao L, Zhang B (2017) Doxorubicin induces cardiotoxicity through upregulation of death receptors mediated apoptosis in cardiomyocytes. Sci Rep 7:44735. https://doi.org/10.1038/srep44735

Zhou T, Zhou X, Xing D (2014) Controlled release of doxorubicin from graphene oxide based charge-reversal nanocarrier. Biomaterials 35:4185–4194. https://doi.org/10.1016/j.biomaterials.2014.01.044